Conf-771204--3

Third IFIP Conference on Computing Methods in Applied Science and Engineering

Versailles, France

December 1977

DISCLAIMER

NUMERICAL CALCULATION OF TRANSONIC FLOW PAST A SWEPT WING BY A FINITE VOLUME METHOD *

Antony Jameson
Courant Institute of Mathematical Sciences, New York University
New York, N. Y. 10012

Conf-771204--3

1. INTRODUCTION

The utility of numerical methods for predicting transonic flows over wings and bodies is by now well established. The computer program FLO22, based on a method presented at the 1973 IFIP Symposium on Computing Methods [1], has actually been widely used to calculate the aerodynamic performance of wings of transport aircraft. Provided that a correction is made for the displacement effect of the viscous boundary layer, this code has been found to give predictions which are accurate enough to serve as a useful design guide [2]. The salient features of the code are:

(1) the use of a potential flow approximation to the equations of motion

(2) the use of upwind differencing in the supersonic zone to simulate the region of dependence of the flow, and to prevent the appearance of expansion shock waves which would violate the entropy inequality

(3) the use of a relaxation procedure based on an artificial time dependent equation to solve the difference equations

(4) the use of a curvilinear coordinate system generated by a sequence of simple transformations to produce coordinate surfaces following the wing shape.

The use of the potential flow approximation greatly reduces the amount of computation required. Since the resulting flow is irrotational, it is consistent to approximate shock waves by discontinuities across which entropy is conserved. This approximation has been found quite satisfactory in practice, since the shock waves generated by airplanes cruising at subsonic speeds are generally quite weak. In fact the appearance of stronger shock waves marks the onset of drag rise, which sets an upper bound on the cruising speed. In order to obtain a unique solution to the potential flow equation, it is necessary to

* This work was supported by the Office of Naval Research under Contract N00014-77-C-0032, and also by NASA under Grants NGR 33-016-167 and NGR 33-016-201. The calculations were performed at the ERDA Mathematics and Computing Laboratory, under Contract EY-76-C-02-3077.*000.

exclude expansion shock waves, corresponding to the condition that entropy can only increase. The use of upwind differencing in the supersonic zone, first introduced by Murman and Cole [3], has been found an effective way to enforce the entropy condition. The nonlinear equations generated by the discrete approximation are not easy to solve. The use of a relaxation process modeled on an artificial time dependent equation [4] has been found to give reliable and acceptably fast convergence.

The main disadvantages of the scheme used in FL022 are the use of nonconservative difference formulas, which result in a failure to satisfy conservation of mass across shock waves, and the difficulty of finding suitable transformations of coordinates to permit the treatment of more complex geometric configurations. The method to be described here is an attempt to overcome these shortcomings, while retaining the successful features of the previous method. The basic idea is to use a discrete approximation which directly represents a balance of the mass flow through small volume elements. This leads to a relatively simple treatment of the potential flow equation in conservation form. The volume elements are distorted cubes generated by local trilinear transformations defined by the element vertices. Elements of this kind can be packed around any reasonably smooth configuration. The subsonic difference formulas can conveniently be derived from the Bateman variational principle [5]. A directional bias is introduced in the supersonic zone by adding an artificial viscosity, which is constructed in such a way as to produce an effective switch to upwind differencing. This serves to prevent the appearance of expansion shock waves. The artificial viscosity has a divergence form, so that the conservation form of the equations is preserved by the difference scheme, and proper shock jump relations, consistent with the isentropic approximation, are satisfied in the limit as the mesh width is decreased to zero [6]. The most promising alternative to the use of artificial viscosity to enforce the entropy condition appears to be the optimal control method proposed by Glowinski and Pironneau [7], in which the entropy condition is represented by penalty functions.

2. FORMULATION OF THE EQUATIONS

The flow is assumed to be isentropic and to satisfy the equations of potential flow. Let $\underset{\sim}{q}$ be the velocity vector, with magnitude q, and ρ the density. Then the potential flow equation can be written in conservation form as

(1) $$\nabla \cdot (\rho \underset{\sim}{q}) = 0$$

where $\underset{\sim}{q}$ is the gradient of the potential .

(2) $$\underset{\sim}{q} = \nabla \phi$$

Let a be the local speed of sound, and M the Mach number q/a. Also let M_∞ , $q_\infty = 1$ and $\rho_\infty = 1$ be the Mach number, speed and density of the uniform flow at infinity. Then the local density is given by the formula

(3) $$\rho = \left\{1 + \frac{\gamma-1}{2} M_\infty^2 (1 - q^2)\right\}^{1/(\gamma-1)}$$

where γ is the ratio of specific heats, and the pressure and speed of sound follow from the relations

(4) $$p = \frac{\rho^\gamma}{\gamma M_\infty^2} , \qquad a^2 = \frac{\rho^{\gamma-1}}{M_\infty^2}$$

Equation (1) is hyperbolic in supersonic flow (M > 1) and elliptic in subsonic flow, and shock waves will generally appear if there is a region of supersonic flow. The shock jump conditions are

(a) continuity of ϕ implying continuity of the tangential velocity component

(b) continuity of ρq_n , where q_n is the normal velocity component

(c) the entropy condition that q_n decreases through the shock.

Under the assumption of isentropic flow, conditions (a) and (b) imply that the normal component of momentum is not conserved. The resulting momentum deficiency causes the appearance of a drag force, which is an approximation to the wave drag [8].

The boundary condition at the body is

(5) $$q_n = \frac{\partial \phi}{\partial n} = 0$$

To obtain a unique lifting solution we also impose the Kutta condition that the flow leaves the trailing edge smoothly with equal velocities along the upper and lower surfaces. The resulting spanwise variation in the circulation $\Gamma = \int q \, ds$ around each section of the wing causes a vortex sheet to be shed from the trailing edge. The vortex sheet will be convected with the flow, and roll up along its side edges. In the calculations this will be ignored and the vortex sheet will be assumed to coincide with a coordinate surface. The conditions applied

at the sheet are then

(a) the jump Γ in the potential is constant along lines parallel to the free stream

(b) the normal velocity component q_n is continuous through the shock.

According to an analysis of the asymptotic behavior of the potential in the far field [9], ϕ approaches the potential of the undisturbed uniform flow except in the Trefftz plane far downstream, where it satisfies the two dimensional Laplace equation for the flow induced by the vortex sheet.

In a finite domain R with boundary S equations (1)-(5) are equivalent to the Bateman variational principle that

$$I = \int_R p \, dR \tag{6}$$

is stationary. In fact according to equations (3) and (4), a variation $\delta\phi$ causes a variation

$$\delta p = - \rho \underset{\sim}{q} \cdot \delta \underset{\sim}{q}$$

Thus

$$\delta I = - \int_R \rho \underset{\sim}{q} \cdot \nabla \, \delta\phi \, dR$$

$$= \int_R \delta\phi \, \nabla \cdot (\rho \underset{\sim}{q}) \, dR - \int_S \delta\phi \, \rho \, q_n \, ds$$

and the boundary terms vanish if $\delta\phi = 0$ or $q_n = 0$.

NUMERICAL SCHEME

The Bateman variational principle will be used to derive difference formulas through the introduction of a discrete approximation to the integral I defined by equation (6). This leads to a central difference scheme. When such a scheme is used to compute the flow past a profile with fore and aft symmetry, such as an ellipse, the fore and aft symmetry is preserved in the solution, and expansion shocks will appear in transonic flow. Thus any scheme which is not desymmetrized in some way is restricted to subsonic flow. The basic difference formulas will therefore be modified by the addition of artificial viscosity to introduce the desired directional bias in the supersonic zone.

In order to represent the Bateman integral, the region in which the flow is to be computed is divided into distorted cubic cells,

generated from cubes by separate transformations between local coordinates X,Y,Z and Cartesian coordinates x,y,z, as illustrated in Figure 1.

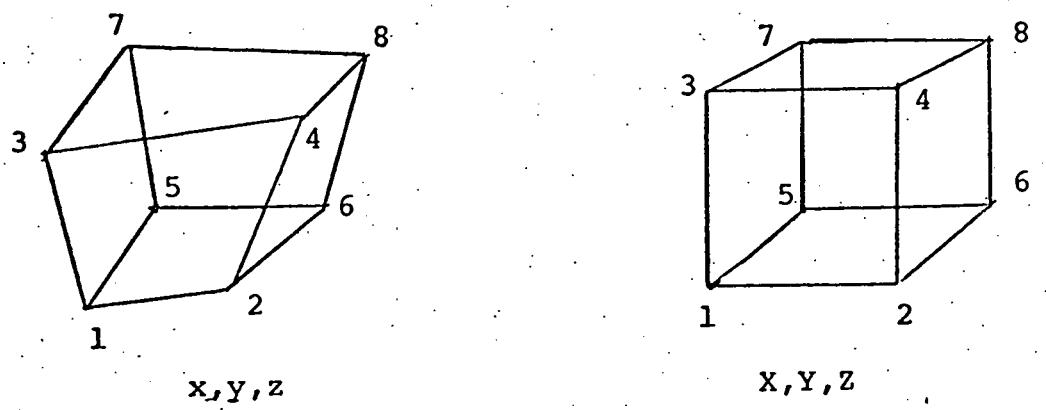

Figure 1

The vertices of the cells define the computational mesh, and subscripts i,j,k will be used to denote the value of a quantity at a mesh point. In order to reduce the amount of computation a simple one point integration scheme will be used, in which the contribution of each cell to the integral will be evaluated as the pressure at the cell center (defined as the point mapped from the center of the cube in the X,Y,Z coordinate system) multiplied by the cell volume. Quantitites evaluated at the cell centers will be denoted by subscripts i+1/2, j+1/2, k+1/2. Averaging and difference operators will be introduced through the notation

$$\mu_X f_{i,j,k} = \frac{1}{2}\left(f_{i+1/2,j,k} + f_{i-1/2,j,k}\right)$$

$$\delta_X f_{i,j,k} = f_{i+1/2,j,k} - f_{i-1/2,j,k}$$

It will also be convenient to use notations such as

$$\mu_{XX} f = \mu_X(\mu_X f) , \qquad \mu_{XY} f = \mu_X(\mu_Y f)$$

$$\delta_{XX} f = \delta_X(\delta_X f) , \qquad \delta_{XY} f = \delta_X(\delta_Y f)$$

Numbering the vertices of a particular cell from 1 to 8 as in Figure 1, the vertices in the local coordinates are assumed to be at $X_i = \pm\frac{1}{2}$, $Y_i = \pm\frac{1}{2}$, $Z = \pm\frac{1}{2}$. If x_i, y_i, z_i are the Cartesian coordinates of the i^{th} vertex, the local mapping is then defined by the trilinear form

$$x = 8 \sum_{i=1}^{8} x_i \left(\frac{1}{4} + X_i X\right)\left(\frac{1}{4} + Y_i Y\right)\left(\frac{1}{4} + Z_i Z\right) \tag{7}$$

with similar formulas for y, z. The potential is assumed to have a similar form inside the cell

$$\phi = 8 \sum_{i=1}^{8} \phi_i \left(\frac{1}{4} + X_i X\right)\left(\frac{1}{4} + Y_i Y\right)\left(\frac{1}{4} + Z_i Z\right) \tag{8}$$

These formulas preserve the continuity of x,y,z and ϕ at the cell boundaries because the mappings in each cell reduce to the same bilinear form at the common face. At the cell center the derivatives of the transformation can be evaluated by formulas such as

$$x_X = \frac{1}{4}\left(x_2 - x_1 + x_4 - x_3 + x_6 - x_5 + x_8 - x_7\right) = \mu_{YZ}\delta_X x$$

Similarly it follows from equation (8) that

$$\phi_X = \mu_{YZ}\delta_X\phi \ , \quad \phi_{XY} = \mu_Z\delta_{XY}\phi \ , \quad \phi_{XYZ} = \delta_{XYZ}\phi$$

In order to evaluate the contribution of each cell to the Bateman integral it is now necessary to express the pressure and cell volume in terms of the local derivatives of the mapping and the potential. Let H be the transformation matrix

$$H = \begin{bmatrix} x_X & x_Y & x_Z \\ y_X & y_Y & y_Z \\ z_X & z_Y & z_Z \end{bmatrix} \tag{9}$$

and let h be the determinant of H. Then the metric tensor is defined by the matrix

$$G = H^T H \tag{10}$$

Also the contravariant velocity components are U,V,W where

$$\begin{bmatrix} U \\ V \\ W \end{bmatrix} = G^{-1} \begin{bmatrix} \phi_X \\ \phi_Y \\ \phi_Z \end{bmatrix} \tag{11}$$

Then

$$q^2 = U\phi_X + V\phi_Y + W\phi_Z$$

and the variation in p due to a variation $\delta\phi$ is

$$\delta p = -\rho\delta\left(\frac{q^2}{2}\right) = -\rho\left(U\delta\phi_X + V\delta\phi_Y + W\delta\phi_Z\right)$$

According to the one point integration scheme, the contribution from the cell centered at i+1/2, j+1/2, k+1/2 is the volume of the cell, given by the determinant $h_{i+1/2,j+1/2,k+1/2}$, multiplied by the pressure $p_{i+1/2,j+1/2,k+1/2}$. On setting

$$\frac{\partial I}{\partial \phi_{i,j,k}} = 0$$

and collecting the contributions from the 8 cells with a common vertex i,j,k, we then obtain the formula

$$\mu_{YZ}\delta_X(\rho hU) + \mu_{ZX}\delta_Y(\rho hV) + \mu_{XY}\delta_Z(\rho hW) = 0 \tag{12}$$

at each interior mesh point. Along the boundary there are only 4 cells adjacent to each mesh point, and equation (12) is correspondingly modified.

Equation (12) is a discrete approximation to the conservation law

$$\frac{\partial}{\partial X}(\rho hU) + \frac{\partial}{\partial Y}(\rho hV) + \frac{\partial}{\partial Z}(\rho hW) \tag{13}$$

which can be derived directly from equation (1) by using the tensor formula for the divergence operator [9]. In fact we can derive equation (12) by representing a flux balance through a set of auxiliary cells, each of which is generated from a cube joining the centers of 8 primary cells, as illustrated in Figure 2.

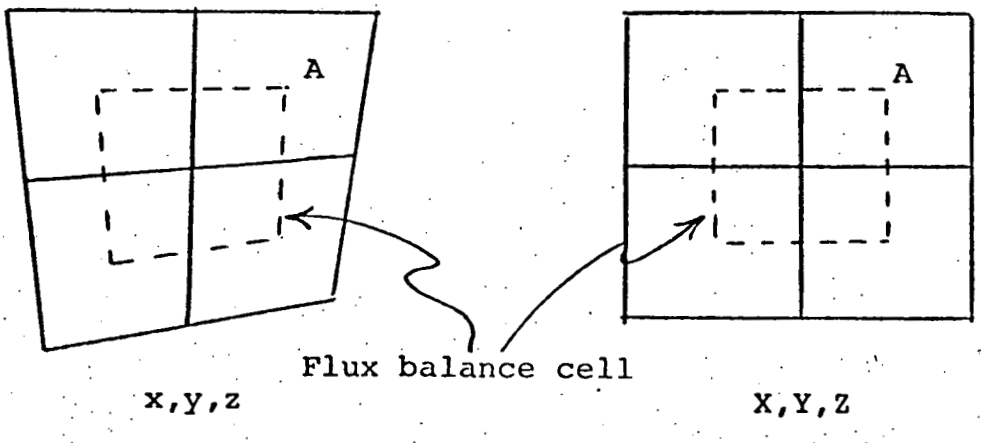

Figure 2

In this interpretation $(\rho hU)_{i+1/2,j+1/2,k+1/2}$ is an approximation to the flux across the face X - 0 of that part of the secondary cell which lies in the primary cell A in Figure 2. The boundary condition (5) reduces to U = 0, V = 0 or W = 0 on cell faces which coincide with the boundary. The flux balance is then represented with secondary cells bounded on one or more faces by the body surface, as illustrated in Figure 3.

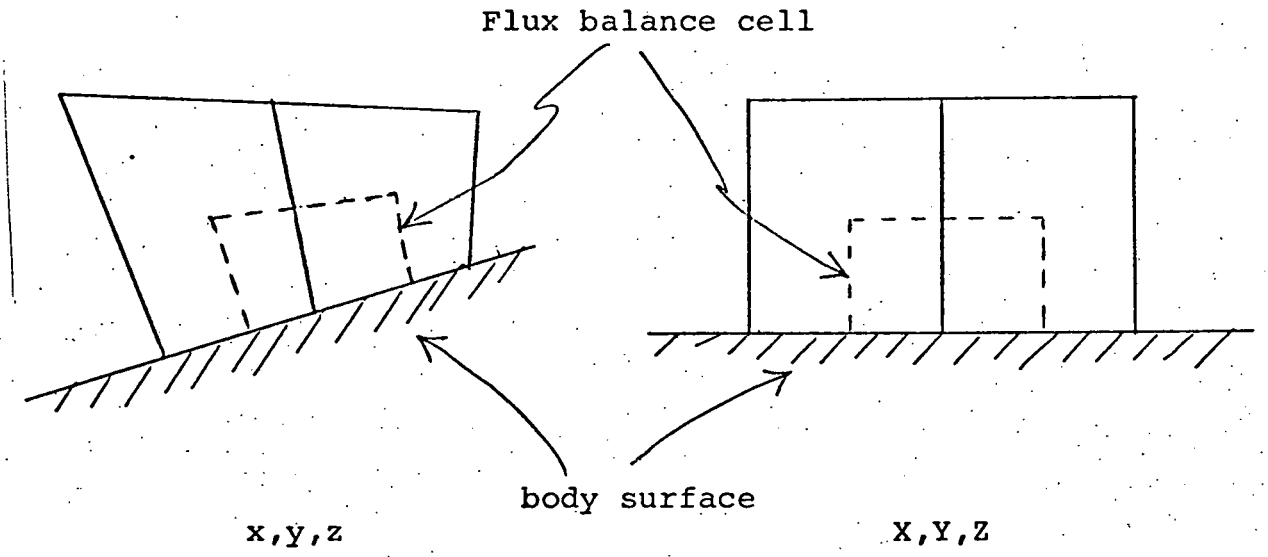

Figure 3

The lumping error introduced by the one point integration scheme now appears as an error introduced by calculating ρ, h, U, V, W at the corners of each secondary cell, instead of averaging these quantities over the cell faces. If the vertices of the primary cells are generated by a global mapping smooth enough to allow Taylor series expansions of x,y,z as functions of X,Y,Z, then the contributions to this error from adjacent primary cells offset each other, with the result that equation (12) approximates equation (13) with a second order local discretization error.

The one point integration scheme has another disadvantage, however, which can be seen from the following simple example. Setting h = 1, ρ = 1, equation (12) reduces in the two dimensional case to

$$(\mu_{YY}\delta_{XX} + \mu_{XX}\delta_{YY})\phi = 0$$

which is the rotated Laplacian scheme

$$\phi_{i+1,j+1} + \phi_{i-1,j+1} + \phi_{i+1,j-1} + \phi_{i-1,j-1} - 4\phi_{ij} = 0$$

The odd and even points are decoupled, so that high frequency oscillations in which $\phi = 1$ at odd points and -1 at even points are admitted by the scheme. To overcome this difficulty we can shift the point of evaluation of the flux ϕ_X across the side AB in Figure 4 from A towards the center of the side by adding a compensating term $- \varepsilon\phi_{XY}$.

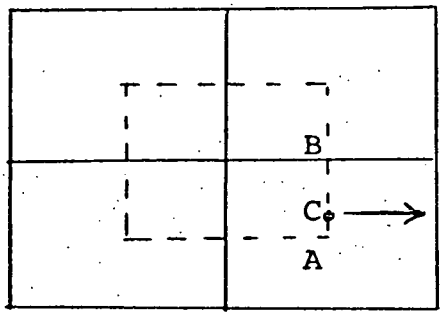

Flux at C is

$(\phi_X)_A + \varepsilon\phi_{XY}$

Figure 4

The addition of similar terms on all faces produces the formula

$$(\mu_{YY}\delta_{XX} + \mu_{XX}\delta_{YY} - \varepsilon\delta_{XYXY})\phi = 0$$

which reduces to the usual 5 point second order accurate formula when $\varepsilon = 1/2$, and to the 9 point fourth order accurate formula when $\varepsilon = 1/3$.

Similarly in the discrete approximation to equation (13) we want to prevent excessive spatial averaging in the approximation of $\phi_{XX}, \phi_{YY}, \phi_{ZZ}$. Allowing for the dependence of ρ on ϕ_X, ϕ_Y, ϕ_Z, the coefficients of $\phi_{XX}, \phi_{YY}, \phi_{ZZ}$ in equation (13) are

$$A_X = \rho h(g^{11} - U^2/a^2)$$
$$A_Y = \rho h(g^{22} - V^2/a^2)$$
$$A_Z = \rho h(g^{33} - W^2/a^2)$$

where g^{ij} are the elements of G^{-1}. In order to compensate equation (12), we can use these coefficients to determine the magnitude of the terms which should be added to shift the locations at which ϕ_X, ϕ_Y, ϕ_Z are effectively evaluated in calculating the fluxes across each face, for example, $\varepsilon A_X \mu_Z \delta_{XY}\phi$ to shift ϕ_X in the Y direction. Collecting the contributions from each of the 8 primary cells surrounding a mesh point, we obtain the following formulas. Let

$$Q_{XY} = (A_X + A_Y)\mu_Z \delta_{XY}\phi$$

with similar formulas for Q_{YZ} , Q_{ZX} , and let

$$Q_{XYZ} = (A_X + A_Y + A_Z)\delta_{XYZ}\phi$$

Then the final compensated equation is

$$(14)\quad \mu_{YZ}\delta_X(\rho hU) + \mu_{ZX}\delta_Y(\rho hV) + \mu_{XY}\delta_Z(\rho hW) - \varepsilon\{\mu_Z\delta_{XY}Q_{XY} + \mu_X\delta_{YZ}Q_{YZ} + \mu_Y\delta_{ZX}Q_{ZX} - \frac{1}{2}\delta_{XYZ}Q_{XYZ}\} = 0$$

where $0 \leq \varepsilon \leq 1/2$. In practice the value $\varepsilon = 1/2$ has been used.

It remains to add the artificial viscosity required to desymmetrize the scheme in the supersonic zone. Instead of equation (13) we shall satisfy the modified conservation law

$$\frac{\partial}{\partial X}(\rho hU+P) + \frac{\partial}{\partial Y}(\rho hV+Q) + \frac{\partial}{\partial Z}(\rho hW+R) = 0$$

where the added fluxes P,Q,R are proportional to the cell widths in the physical domain, with the result that the correct conservation law is recovered in the limit as the cell width is reduced to zero. The artificial viscosity is designed to produce an effective switch to upwind differencing in the supersonic zone. Presuming the distribution of mesh points to be smooth, it is constructed in the following manner. First we introduce the switching function

$$\mu = h \max\left\{0, \left(1 - \frac{a^2}{q^2}\right)\right\}$$

and we construct $\hat{P}$ by the formula

$$\hat{P} = \mu \frac{\rho}{a^2}\left(U^2\delta_{XX} + UV\mu_{XY}\delta_{XY} + WU\mu_{ZX}\delta_{ZX}\right)\phi$$

and $\hat{Q}$, $\hat{R}$ by similar formulas. Then

$$P_{i+1/2,j,k} = \begin{cases} \hat{P}_{i,j,k} & \text{if } U > 0 \\ -\hat{P}_{i+1,j,k} & \text{if } U < 0 \end{cases}$$

with similar shifts for Q, R. Finally, equation (14) is modified by the addition of

$$\delta_X P + \delta_Y Q + \delta_Z R$$

Since $\mu = 0$ when $q < a$, P,Q,R vanish in the subsonic zone. In the supersonic zone they approximate $-\mu|U|\delta_X\rho$, $-\mu|V|\delta_Y\rho$, $-\mu|W|\delta_Z\rho$. It may be verified [11] that the coefficients of the third derivatives of the potential such as ϕ_{XXX}, ϕ_{YXX}, ϕ_{ZXX} introduced by P,Q,R are the same as in the artificial viscosity generated by the rotated difference scheme which has been previously used in three dimensional transonic flow calculations [1,2,4].

Finally the nonlinear equations generated by this discretization process are solved by a generalized relaxation method which is derived by embedding the steady state equation in an artificial time dependent equation. Thus we solve a discrete approximation to

$$\frac{\partial}{\partial X}(\rho hU+P) + \frac{\partial}{\partial Y}(\rho hV+Q) + \frac{\partial}{\partial Z}(\rho hW+R)$$

$$= \alpha\phi_{XT} + \beta\phi_{YT} + \gamma\phi_{ZT} + \delta\phi_T ,$$

where the coefficients α,β,γ are chosen to make the flow direction timelike, as in the steady state equation, and δ controls the damping [4].

4. CONSTRUCTION OF THE MESH

The formulation of the artificial viscosity presupposes a smooth distribution of cells. Also the one point integration scheme will cause a loss of accuracy if the mesh is not smooth. It is important, therefore, to use a reasonably smooth mesh. This is most easily accomplished by using global mappings to generate the mesh points. All other steps, such as the transformation of the equations of motion, are then taken over by the numerical scheme.

Swept wing calculations have been performed on a mesh generated by a sheared parabolic coordinate system, which has been found to give good results with earlier methods [1,2,4]. First, we introduce parabolic coordinates in planes containing the wing section by the transformation

$$\bar{X} + i\bar{Y} = \{[x - x_0(z) + i(y - y_0(z))]/t(z)\}^{1/2}$$

$$\bar{Z} = z$$

where z is the spanwise coordinate, $x_0(z)$ and $y_0(z)$ define a singular line just inside the leading edge, and $t(z)$ is a scaling factor which

can be used to control the number of cells covering the wing.

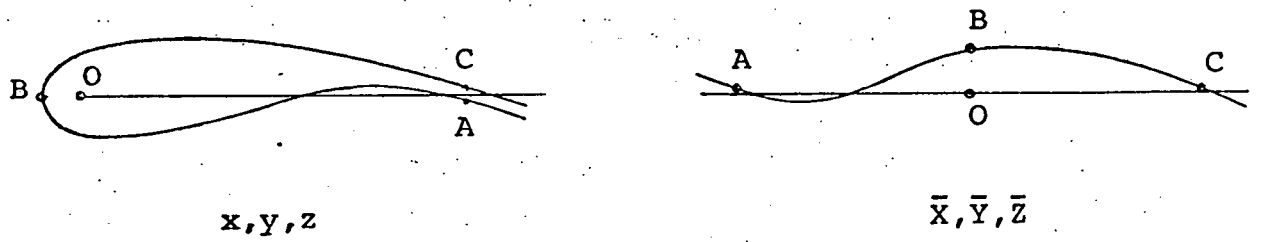

Figure 5

The effect of this transformation is to unwrap the wing to form a shallow bump $Y = S(\bar{X},\bar{Z})$, as illustrated in Figure 5. Then we use a shearing transformation

$$X = \bar{X} \ , \quad Y = \bar{Y} - S(\bar{X},\bar{Z}) \ , \quad Z = \bar{Z}$$

to map the wing to the surface $Y = 0$. The mesh is now constructed by the reverse sequence of transformations from a rectangular grid in the X,Y,Z coordinate system. The vortex sheet trailing behind the wing is assumed to coincide with the coordinate surface leaving the trailing edge. This mesh can be modified to treat wing cylinder combinations by first mapping the cylinder to a vertical slit by a Joukowsky transformation, as illustrated in Figure 6, and then using the same sequence of transformations to generate a sheared parabolic coordinate around the wing projecting from the slit.

Front view of wing-cylinder combination

Cylinder mapped to vertical slit

Figure 6

An alternative mesh generating scheme for wing fuselage combinations [12] starts by introducing cylindrical coordinates as illustrated in Figure 7.

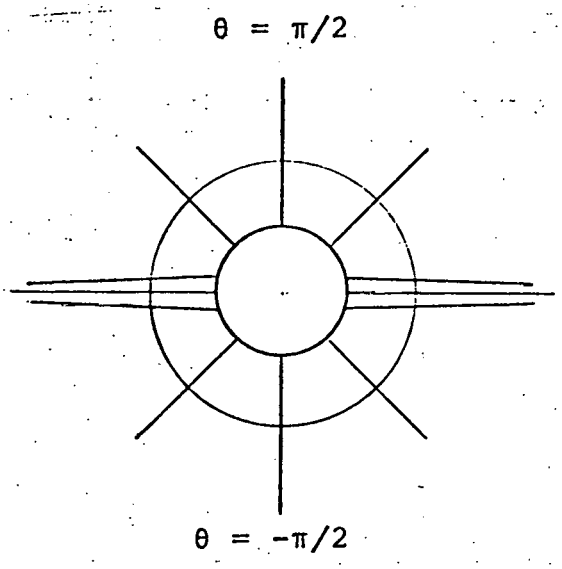

Cylindrical coordinate system for wing body combination

Figure 7

In each cylindrical surface the wing section then appears as a profile in a channel bounded by the intersection of the cylinder with the plane of symmetry at $\theta = \pm \pi/2$. This configuration can be mapped to a channel with a bump on the upper wall, as illustrated in Figure 8, by the transformation

$$\sigma = \log \left(1 - \cosh(\zeta)\right)$$

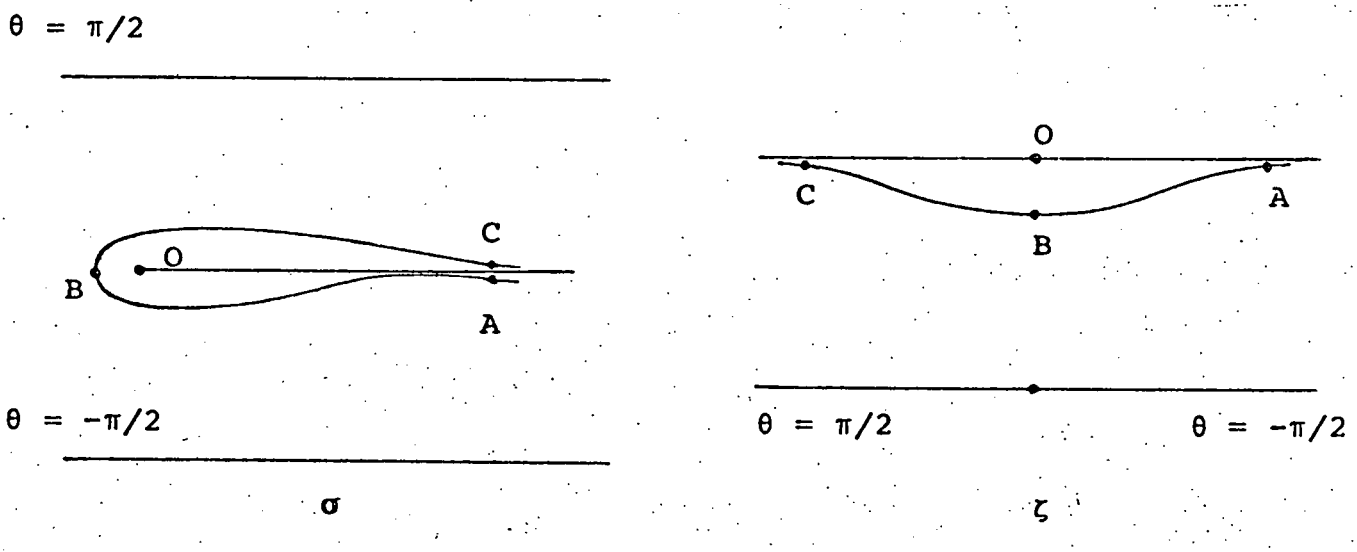

Figure 8

Finally the bump is removed by a shearing transformation.

5. RESULTS

Two examples of numerical calculations are presented in this section to illustrate the capability of the finite volume method. The first mesh generating procedure proposed in Section 4, the sheared parabolic coordinate system, was used in these calculations, both of which were performed on a sequence of three progressively finer meshes. After the calculation on each of the first two meshes, the number of intervals was doubled in each coordinate direction and the interpolated result was used as the starting point for the calculation on the new mesh. The fine mesh contained 160 intervals in the chordwise X direction, 16 intervals in the normal Y direction, and 32 intervals in the spanwise Z direction, for a total of 81,920 cells. 100 relaxation cycles were used on each mesh. Such a calculation takes about 15 minutes on a CDC 7600.

The first example is a calculation of the flow past the ONERA M6 wing, for which experimental data is available [13]. The result is displayed in Figure 9. Separate pressure distributions are shown for stations at 20, 45, 65 and 95 percent of the semispan. Section lift and drag coefficients CL and CD were obtained by integrating the pressure coefficient CP over the profile. The critical pressure coefficient at which the flow has sonic speed is marked by a horizontal line on the pressure axis. Although the calculation did not include a boundary layer correction, it can be seen that the agreement with the experimental data is quite good. The triangular shock pattern is clearly visible in the three dimensional plot of the pressure distribution (Figure 9f). The front shock, emanating from the leading edge at the wing root, merges with the rear shock about three quarters of the way out across the span. The second example is indicative of the level of geometric complexity which can be treated with the existing code. The result is displayed in Figure 10. It is for a Douglas DC 10 wing mounted on a cylinder in a low mid position. The true DC 10 configuration is not exactly modeled, because the code does not provide for a wing root fillet.

These results confirm the promise of the new method. It appears that it can be used to treat configurations of more or less arbitrary complexity, subject to limits set by the power of the available computers. The extension to new configurations is primarily a matter of devising mesh generating schemes, since the internal computations are essentially independent of the configuration, apart from the identification of which elements are the boundary elements.

REFERENCES

1. Jameson, Antony: Three dimensional flows acround airfoils with shocks, IFIP Symposium on Computing Methods in Applied Sciences and Engineering, Versailles, December 1973.

2. Jameson, Antony, and Caughey, D. A.; Numerical calculation of the flow past a swept wing, New York University Report COO-3077-140, June 1977.

3. Murman, E. M., and Cole, J. D.; Calculation of plane steady transonic flows, AIAA Journal, Vol. 9, 1971, pp. 114-121.

4. Jameson, Antony; Iterative solution of transonic flows over airfoils and wings, including flows at Mach 1, Comm. Pure Appl. Math., Vol. 27, 1974, pp. 283-309.

5. Bateman, H.; Notes on a differential equation which occurs in the two dimensional motion of a fluid and the associated variational problem, Proc. Roy. Soc., Series A,, Vol. 125, 1929, pp. 598-618.

6. Lax, Peter,and Wendroff, Burton; Systems of conservation laws, Comm. Pure Appl. Math., Vol. 13, 1960, pp. 217-237.

7. Glowinski, R., and Pironneau, O.; On the computation of transonic flows, Premier Colloque Franco-Japonais d'Analyse Fonctionelle et d'Analyse Numerique, Kyoto, September 1976.

8. Steger, J. L., and Baldwin, B. S.; Shock waves and drag in the numerical calculation of isentropic transonic flow, NASA TN D-6997, 1972.

9. Klunker, E. B., Contribution to methods for calculating the flow about thin lifting wings at transonic speeds -- analytic expressions for the far field, NASA TN D6530, 1971.

0. Synge, J. L., and Schild, A., Tensor Calculus, University of Toronto Press, 1949, pp. 57-58.

11. Jameson, Antony, and Caughey, D. A.; A finite volume method for transonic potential flow calculations, Third AIAA Conference on Computational Fluid Dynamics, Albuquerque, June 1977.

12. Caughey, D. A., and Jameson, Antony, Numerical calculation of transonic potential flow about wing fuselage combinations, AIAA Paper 77-677, AIAA Conference on Plasma an Fluid Dynamics, Albuquerque, June 1977.

13. Monnerie, B., and Charpin, F., Essais de buffeting d'une aile en fleche en transsonique, 10e Colloque d'Aerodynamique Appliquee, Lille, November 1973.

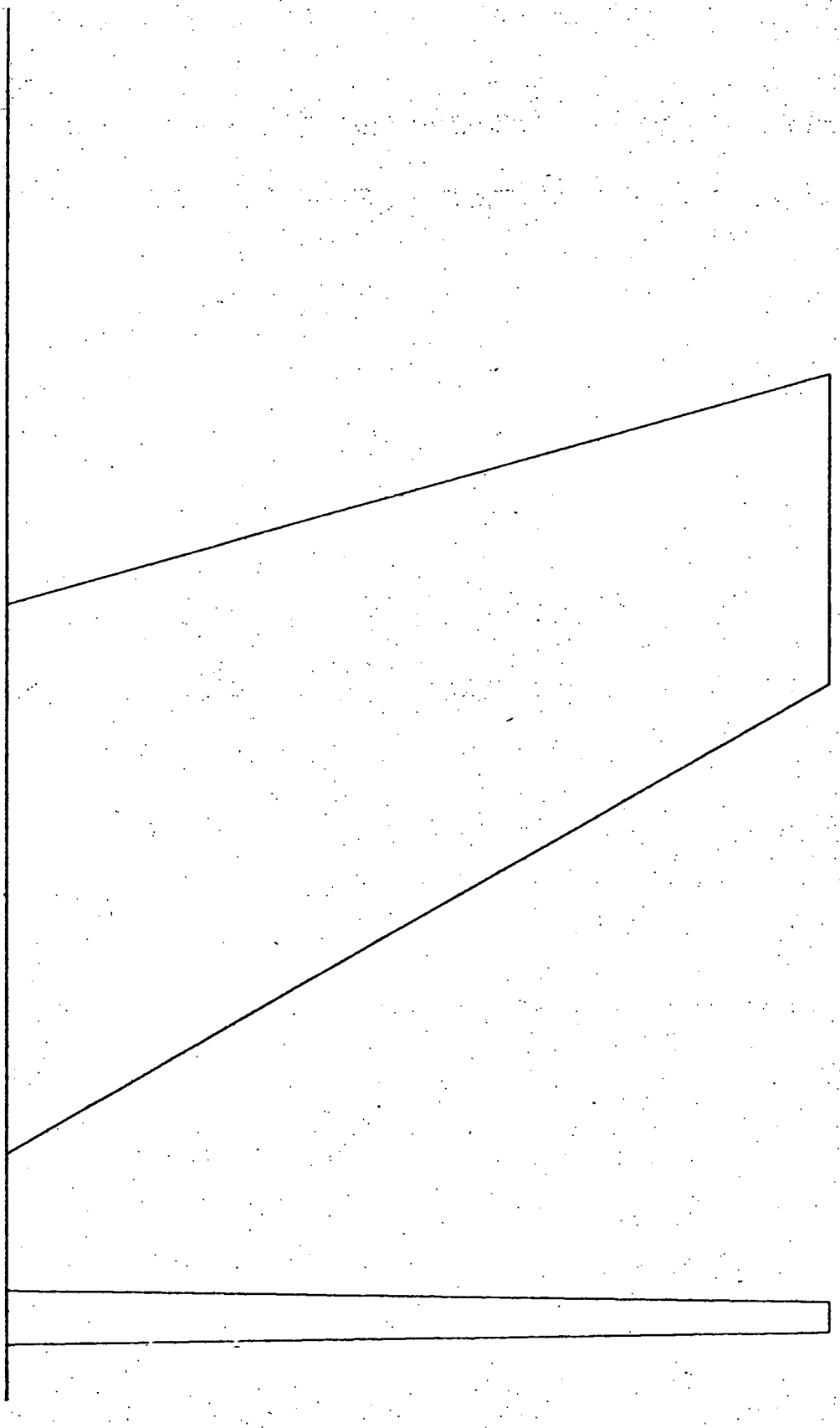

ONERA M6

Figure 9a

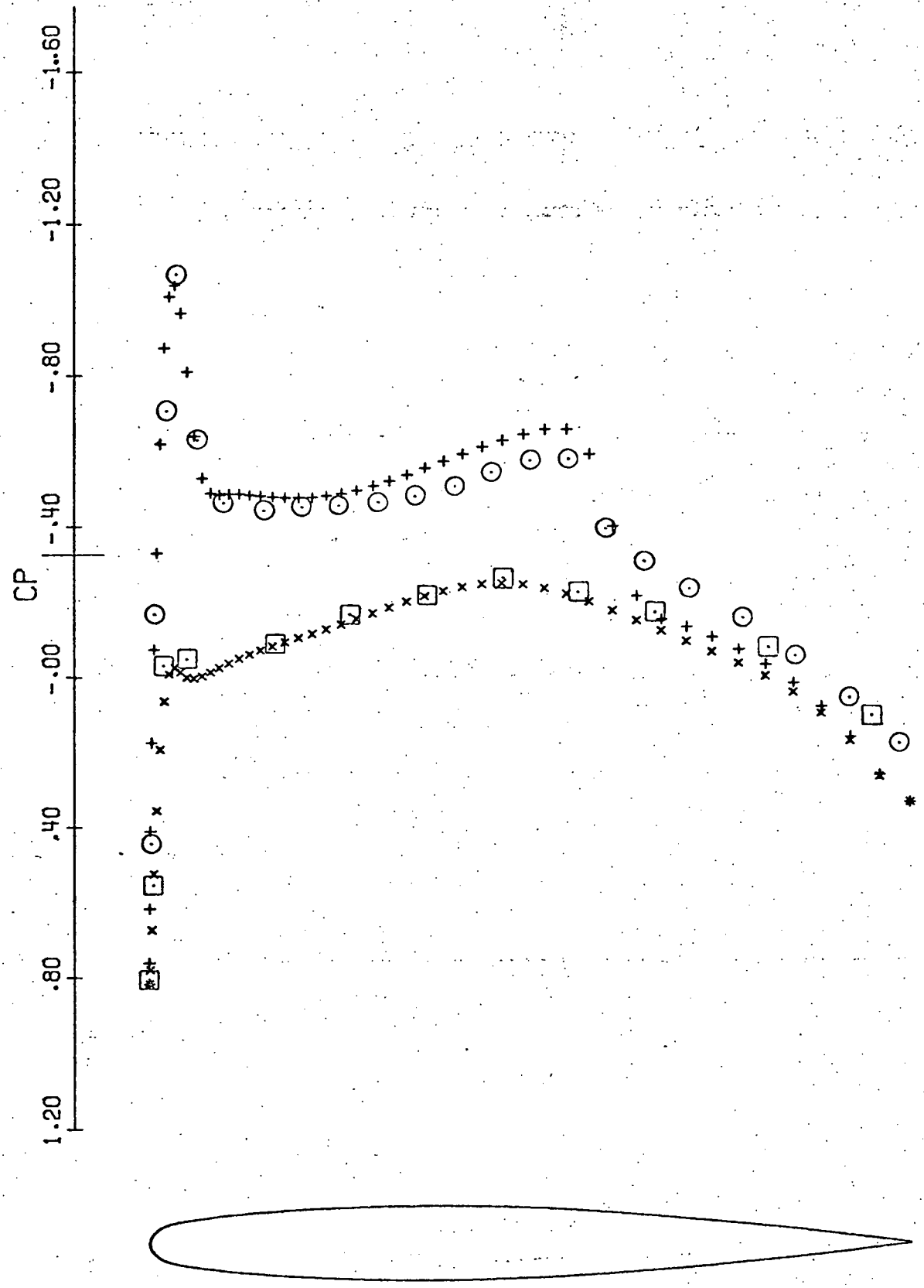

ONERA M6

MACH .840 ANGLE OF ATTACK 3.060°

Z .20 CL .2733 CD .0151

+, × THEORY

O, □ EXPERIMENT

Figure 9b

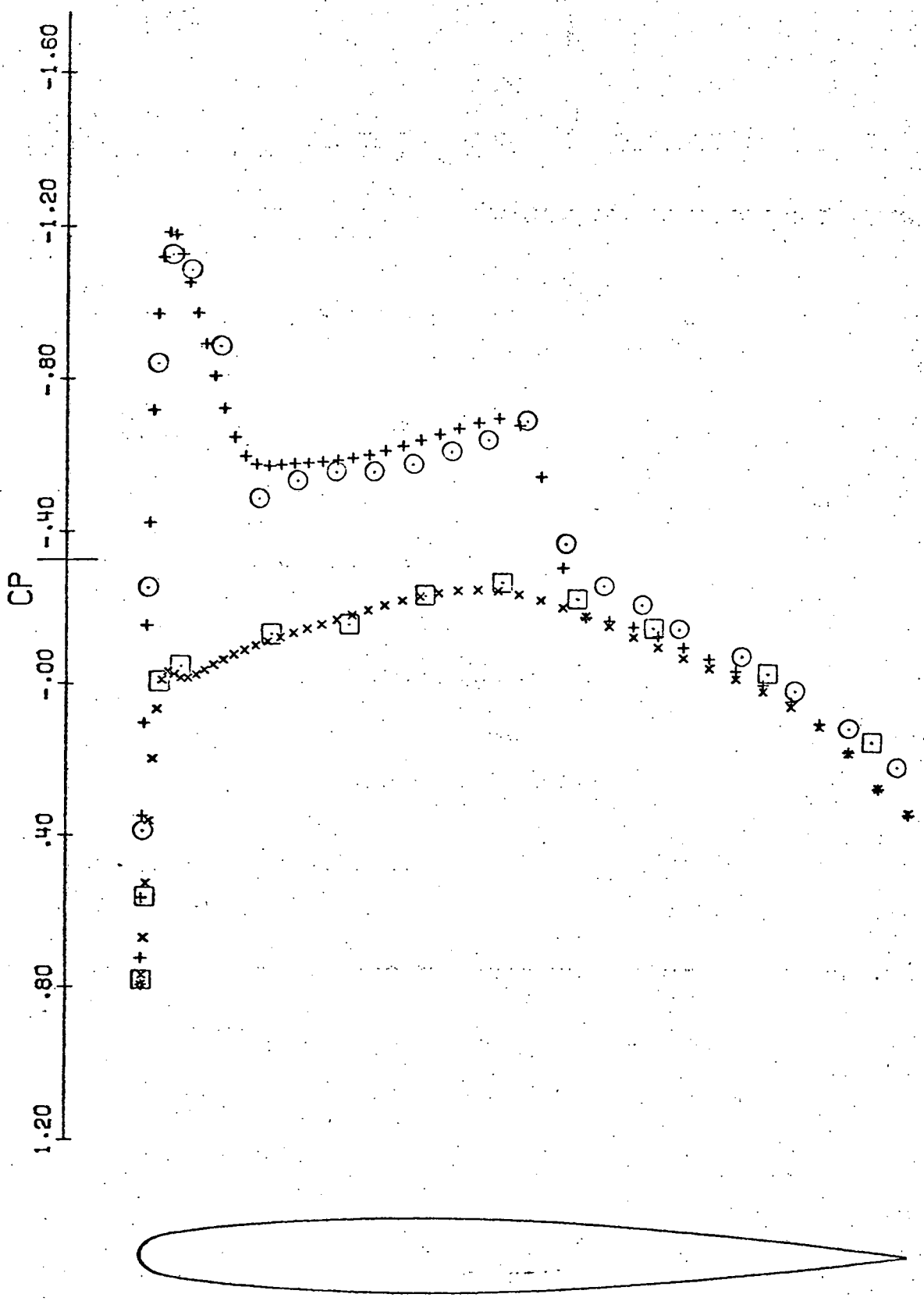

ONERA M6

MACH .840 ANGLE OF ATTACK 3.060°

Z .45 CL .2942 CD .0051

+ , × THEORY

O , □ EXPERIMENT

Figure 9c

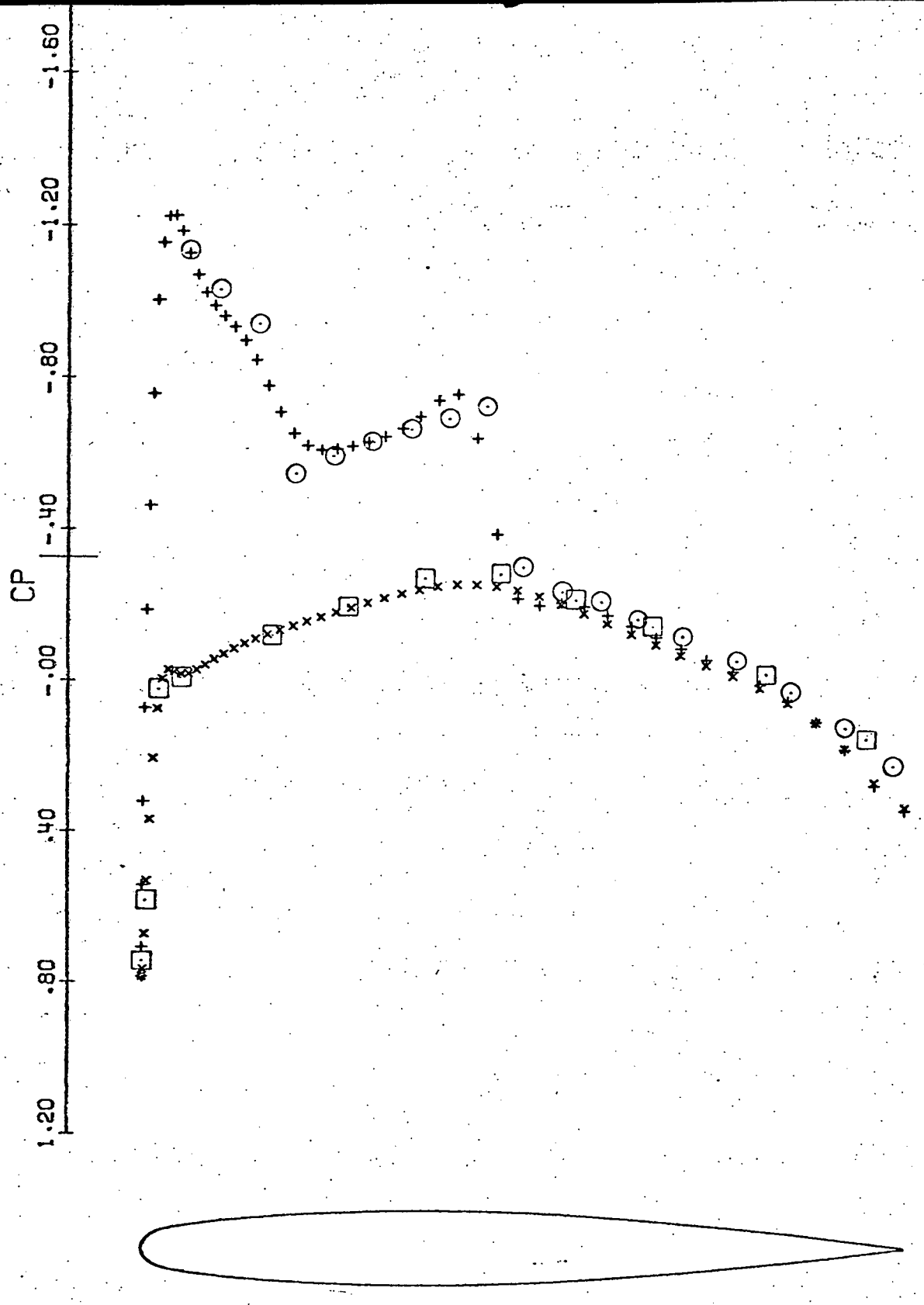

ONERA M6

MACH .840 ANGLE OF ATTACK 3.060°

Z .65 CL .2936 CD -.0006

+ , × THEORY

O , □ EXPERIMENT

Figure 9d

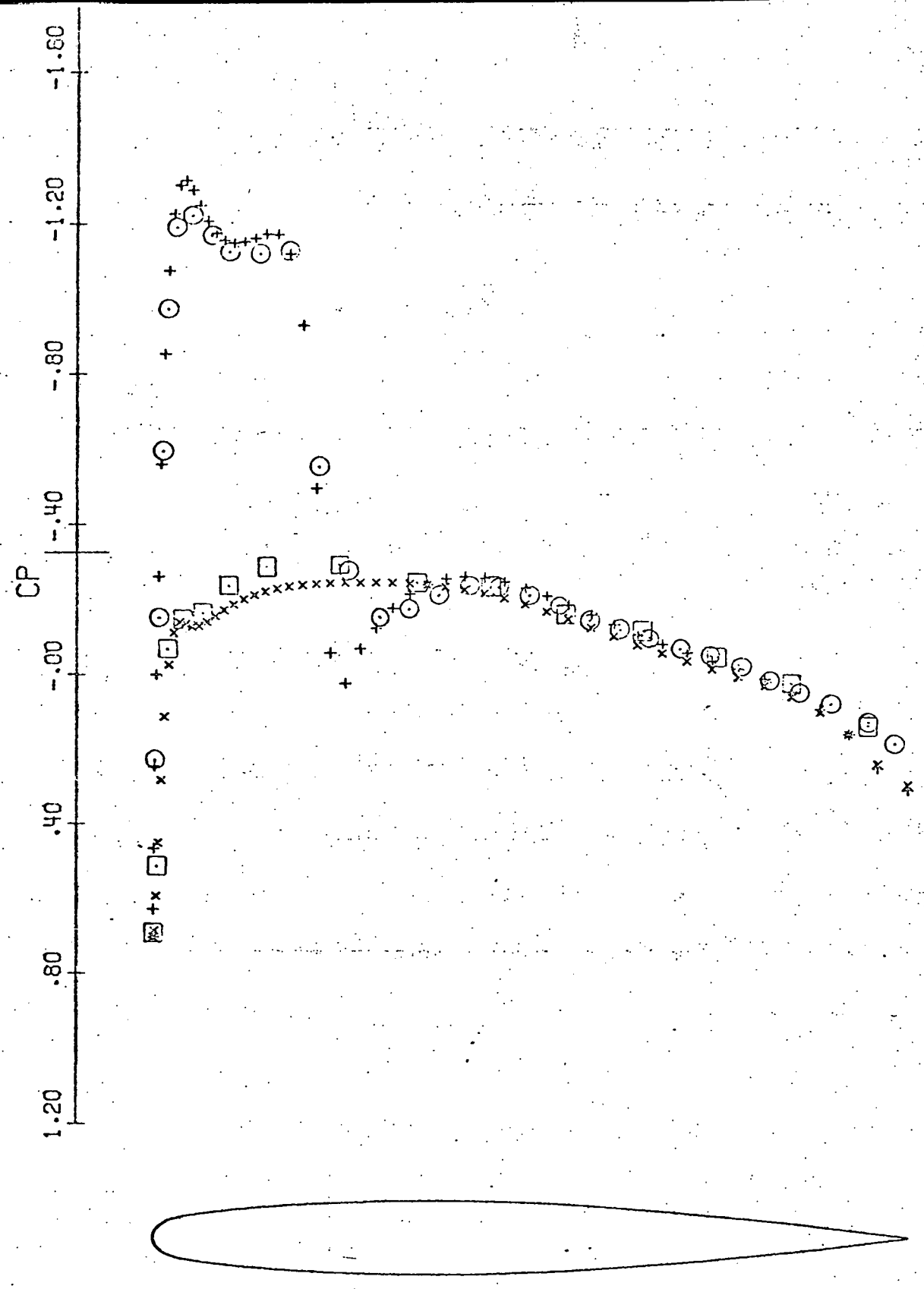

ONERA M6

MACH .840 ANGLE OF ATTACK 3.060°

Z .95 CL .2004 CD -.0148

+ , × THEORY

O , □ EXPERIMENT

Figure 9e

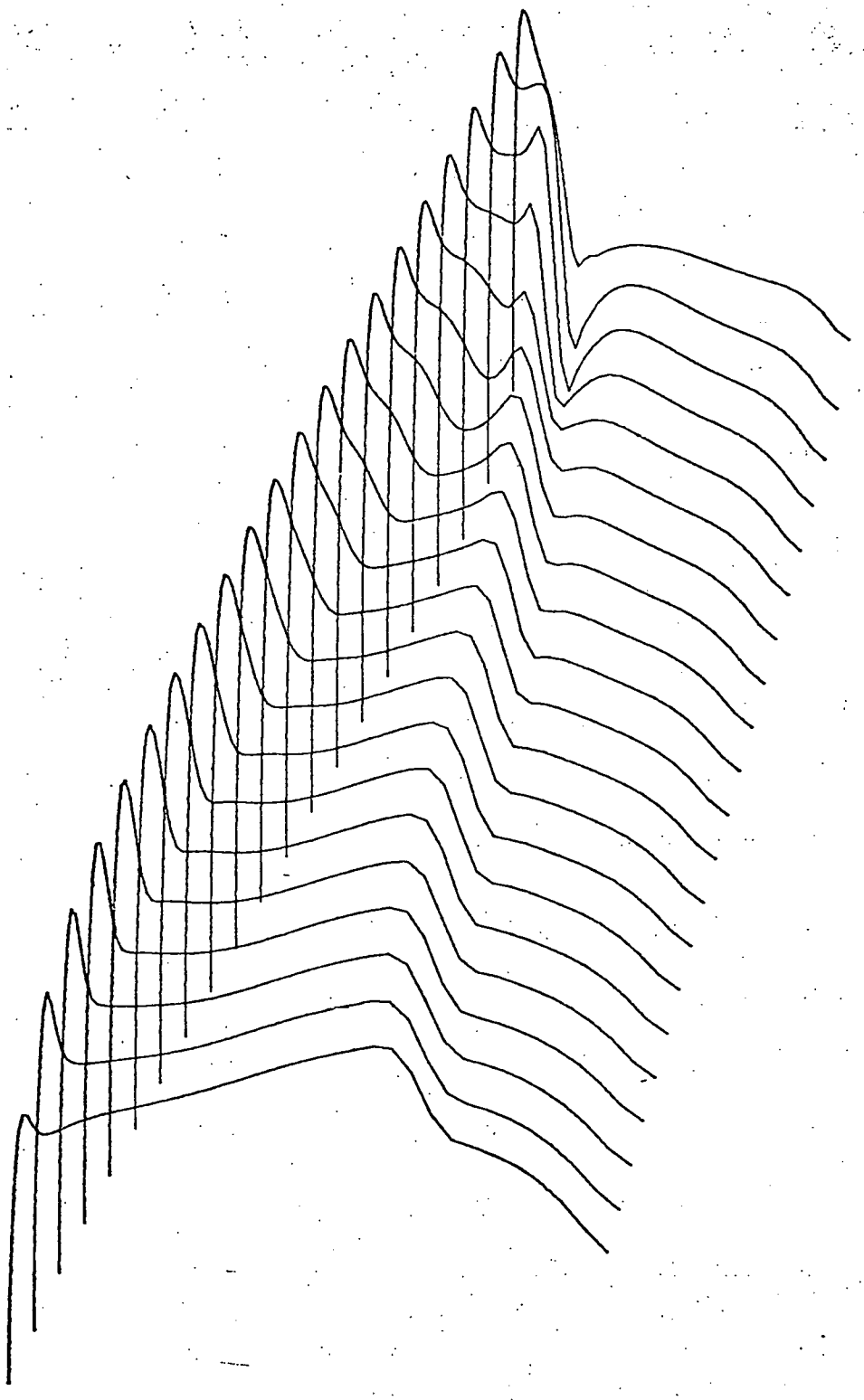

ONERA M6

UPPER SURFACE PRESSURE

MACH .840 ANGLE OF ATTACK 3.060°

Figure 9f

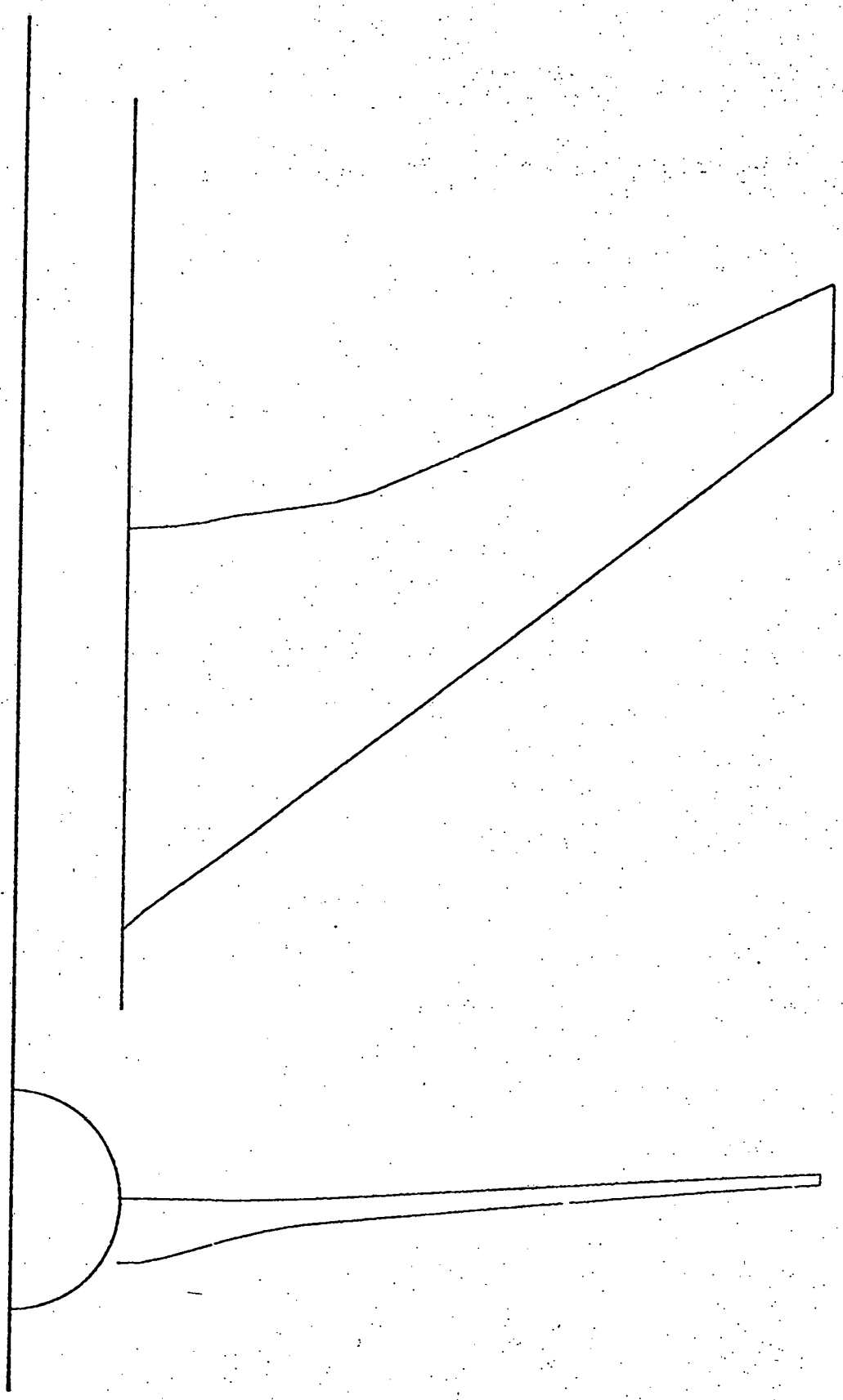

DOUGLAS DC 10

Figure 10a

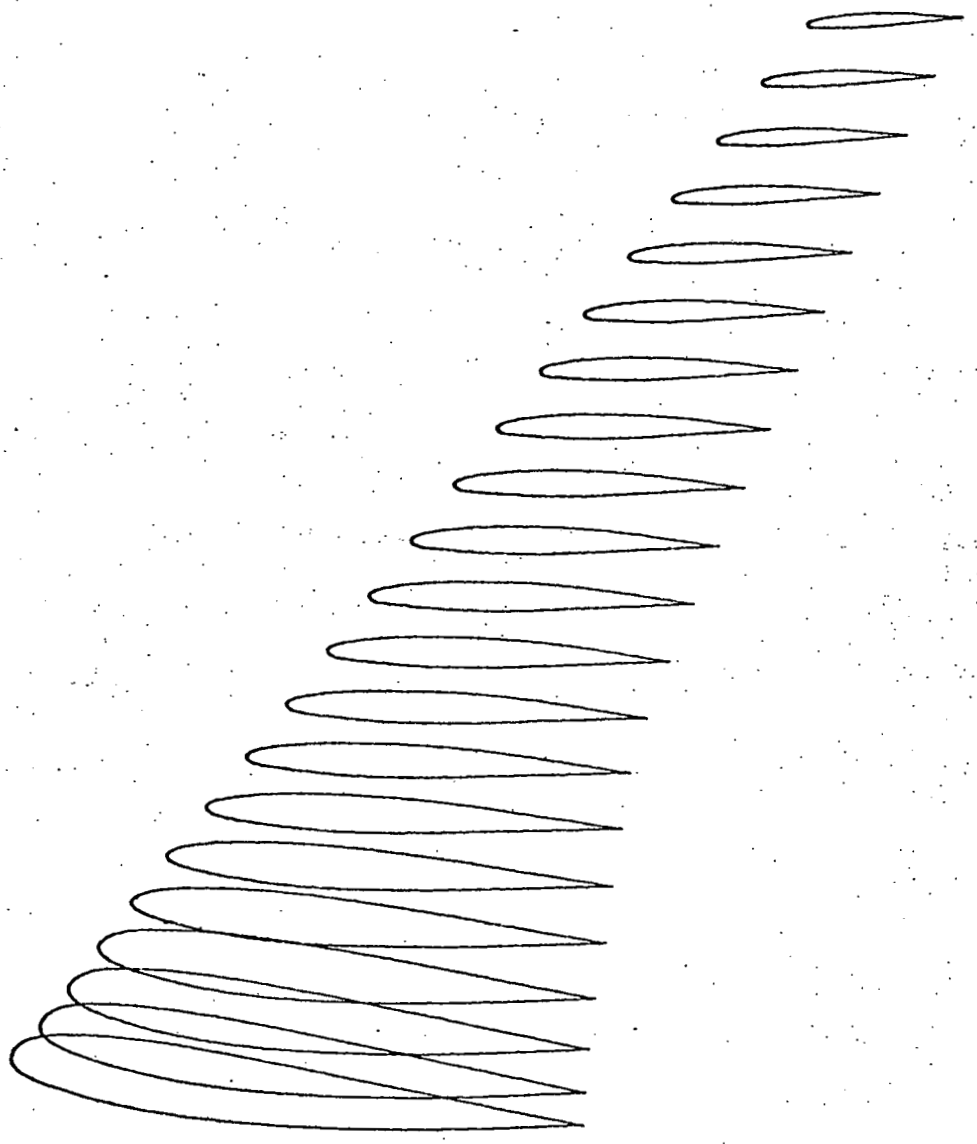

DOUGLAS DC 10

VIEW OF WING

MACH .850 ANGLE OF ATTACK 2.000°

Figure 10b

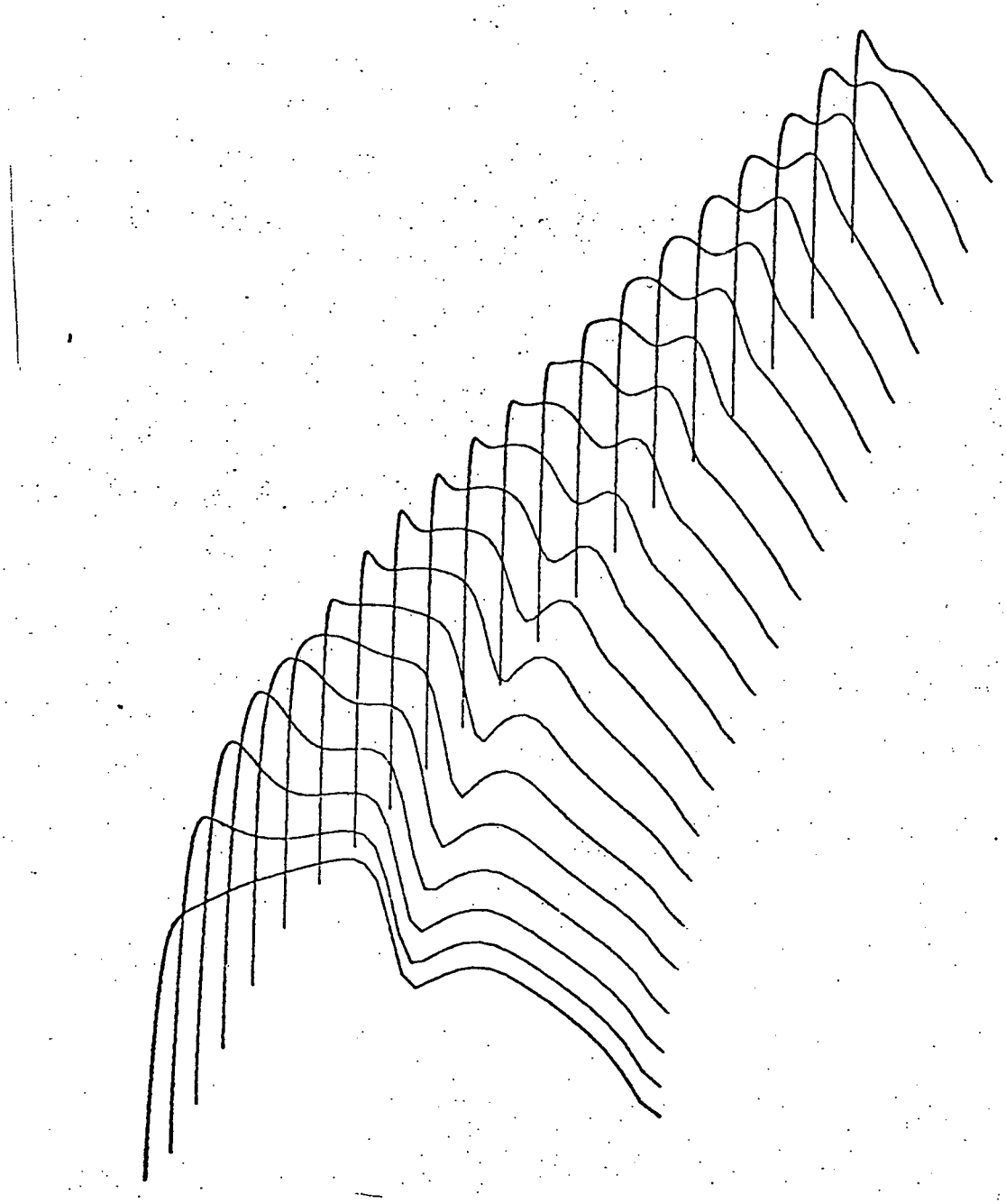

DOUGLAS DC 10

UPPER SURFACE PRESSURE

MACH .850 ANGLE OF ATTACK 2.000°

Figure 10c